HHS Public Access

Author manuscript

Nano Lett. Author manuscript; available in PMC 2019 October 10.

Published in final edited form as:

Nano Lett. 2018 October 10; 18(10): 6604–6610. doi:10.1021/acs.nanolett.8b03235.

Scaling behavior of ionic transport in membrane nanochannels

María Queralt-Martín[#1], **M. Lidón López**[#2], **Marcel Aguilella-Arzo**[2], **Vicente M. Aguilella**[2], and **Antonio Alcaraz**[2,*]

[1]Section on Molecular Transport, Eunice Kennedy Shriver NICHD, National Institutes of Health, Bethesda, Maryland 20892, USA.

[2]Laboratory of Molecular Biophysics, Department of Physics, Universitat Jaume I, Av. Vicent Sos Baynat s/n 12071 Castellón, Spain.

[#] These authors contributed equally to this work.

Abstract

Ionic conductance in membrane channels exhibits a power law dependence on electrolyte concentration ($G \sim c^{\alpha}$). The many scaling exponents α reported in the literature usually require detailed interpretations concerning each particular system under study. Here, we critically evaluate the predictive power of scaling exponents by analyzing conductance measurements in four biological channels with contrasting architectures. We show that scaling behavior depends on several interconnected effects whose contributions change with concentration so that the use of oversimplified models missing critical factors could be misleading. In fact, the presence of interfacial effects could give rise to an apparent universal scaling that hides the channel distinctive features. We complement our study with 3D structure-based Poisson-Nernst-Planck (PNP) calculations giving results in line with experiments and validating scaling arguments. Our findings not only provide a unified framework for the study of ion transport in confined geometries but also highlight that scaling arguments are powerful and simple tools to offer a comprehensive perspective of complex systems, especially those where the actual structure is unknown.

TOC

[*]Author to whom correspondence should be addressed. Phone: +34 964 72 8044., alcaraza@uji.es.

AUTHOR CONTRIBUTIONS

M.Q.M., A.A. and M.L.L performed the electrophysiology experiments and experimental data analysis. M.A.A performed the theoretical calculations. A.A., M.Q.M. and V.M.A. designed the experiments and wrote the manuscript. All authors reviewed the data and edited and approved the final draft of the manuscript.

SUPPORTING INFORMATION

Representative current traces of the different channels studied, at two different electrolyte concentrations. Representative I-V curves of the OmpF and SARS CoV-E channels reconstituted in neutral and charged lipid membranes at different electrolyte concentrations. Experimental methods for membrane formation, ion channel reconstitution, and current recordings. Description and implementation of the three-dimensional Poisson–Nernst–Planck model.

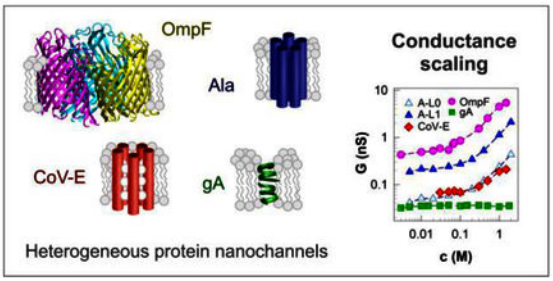

Keywords

scaling behavior; ion transport; biological channel; electrodiffusion; access resistance

Ion permeation through nanometer-sized membrane channels differs significantly from transport in bulk conditions giving rise to striking phenomena like electroneutrality breakdown,[1] local charge inversion,[2,3] tunable ion selectivity[4,5] or energy conversion from electroosmotic effects,[6] among others.[7] Nanoscale confinement is revealed in interfacial effects,[8] entropic interactions,[9,10] van der Waals[11] and other short-range forces.[7] Scaling laws aim at explaining how the size of objects affects their behavior albeit they can describe any functional relationship between two quantities that scale with each other over a significant interval.[12–14] In fact, scaling arguments can be found in economics,[15,16] psychology[17] or to explain human interaction activity[18] among other fields. In this work, we investigate the scaling behavior of channel conductance (G) with salt concentration (c) in biological pores with distinct geometry and charge distribution. Interestingly, a number of previous studies suggest a power law dependence $G \sim c^{\alpha}$ with a large variety of exponents α ranging between 0 and 1 that have been considered as a hallmark of each system, both in synthetic and biological pores.[19–22] We show here that the scaling behavior of these complex systems depends on several interconnected effects, including the influence of the pore intrinsic properties as well as interfacial effects. A theoretical model based on 3D Poisson-Nernst-Planck equations using the actual atomic structure of two protein channels provides a full description of the experiments and confirms our interpretations on the qualitative trends given by scaling laws. By bringing together the scaling behavior of very different ion channels, our findings give a broad perspective of conductance scaling in biological pores and establish a common framework for two contrasting types of membrane channels, the narrow ones key to signaling and neurotransmission and the wide ones involved in keeping cell homeostasis through solute interchange. The notion of a general approach to describe ion transport in pores with dimensions ranging from atomic scale to tenths of nanometers is not only important for protein channels, but it has become extremely relevant in the field of synthetic nanofluidics because in the last years not only channels below the nanoscale have been fabricated,[23–26] but also abiotic nanopores with similar aspect ratios to biological ion channels.[27,28]

Protein and proteolipidic nanopores.

We explore ion transport properties in a variety of biological ion channels that differ in their structure, charge distribution and geometry, as represented in Figure 1. On the one side, we consider channels formed by transmembrane proteins: the narrow Gramicidin A (gA) (r ~ 0.4 nm)[29] and the wide bacterial porin OmpF (three identical pores of r ~ 1–2 nm).[30–34] On the other side, we deal with channels formed by combined assemblies of proteins and lipids (proteolipidic pores): the peptide antibiotic Alamethicin (Ala) forming two types of pores Ala-0 (r ~ 0.75nm), and Ala-1 (r ~ 1.2 nm) among other larger bigger oligomers[35,36] and the SARS Coronavirus Envelope Protein (CoV-E).[37–39]

Experimental scaling of ion conductance.

Figure 2(a) shows conductance (G = I/V) measurements in a wide range of KCl concentration in channels reconstituted into neutral lipid membranes (DPhPC). All G(c) plots display a parallel slope or, in other words, a similar scaling –close to linearity (actually, $G \sim c^{0.8}$)– for a wide range (2 mM - 2 M) of salt concentration (except for gA whose conductance saturates around ~1 M).[40] Interestingly, the common scaling exhibited by such different systems is very similar to that measured for solution conductivity (Figure 2(a), inset). This is surprising for gA, which exhibits single-file transport of partially dehydrated cations[41] despite having in fact almost zero net charge.[42,43] Also, the absence of any charge effects in OmpF, Ala and CoV-E is intriguing. Although they are wide enough to allow the multiionic transport of hydrated ions, they are also known to display considerable ion discrimination at least in the low concentration limit.[36,38,39]

Figure 2(b) reports the values for the conductance measured when channels are reconstituted in negatively charged membranes of diphytanoyl phosphatidylserine (DPhPS). In this case, decreasing salt concentration changes conductance scaling in all channels except for gA. In concentrated solutions (c > 0.1 M), scaling is the same as in neutral membranes (Figure 2(a), $G \sim c^{0.8}$) while in the low c regime, G is independent of salt concentration ($G \sim c^0$). For charged membranes, the latter scaling is displayed by gA in the whole concentration range. Besides, the concentration at which the scaling changes varies with the channel considered, suggesting some intrinsic features of each system.

Results in Figure 2 were obtained at a particular applied potential (+100 mV for OmpF, gA and CoV-E, and +140 mV for Ala), although these results are expected to be voltage-independent. Indeed, previous studies have shown that current rectifications in gA are very weak, and appear only at very high potentials, much larger than the one used here.[44–46] Alamethicin current has been shown to be almost voltage-independent.[47] For the case of OmpF and CoV-E, we have measured IV curves for both neutral and charged lipids at high and low salt concentrations (Figures S2 and S3), showing that there is no rectification in the conditions of our study. Actually, for the case of OmpF, even under a salt concentration gradient the current rectification displayed by the channel is very mild, as shown in Figure S4.

To gain further insight into the factors modulating conductance scaling in Figure 2, we analyze separately two effects that could alter bulk-like ionic transport: membrane charge and protein charge. Figure 3(a) displays G measurements for OmpF (*upper panel*) and gA (*lower panel*) channels, showing that lipid composition determines the actual scaling. Data exhibit scaling exponents between 0 and 1 either in an uncharged narrow channel like gA or in a wide charged channel like OmpF. Note that scaling exponents in Figure 3(a) differ slightly from those reported in Figure 2 because the range of concentration has been shortened to focus on low concentration values where surface effects are expected.

Figure 3(b) shows that protein charge controls the scaling behavior in a similar way as done by membrane charge. The conductance scaling is measured for OmpF inserted in a charged membrane (DPhPS), and protein charges are modulated by changing solution pH. Clearly, channel charge is enough to control ion transport, which can vary from almost bulk conduction ($G \sim c^{0.8}$) when the channel is neutral (its isoelectric point is *ca*. pH 4, at which the channel has no selectivity and displays no current rectification, so it can be considered to have an overall zero net charge)[4,30] to $G \sim c^{0.1}$ at pH 6 when the channel is negatively charged.[30] Note that within this pH range (4–6), membrane charge remains unchanged, because DPhPS lipid polar heads have an effective pKa below 3.[48]

As seen, both protein and lipid charges can control the scaling behavior of G versus c, but it is still unclear whether each factor operates independently, or their effects somewhat interfere. Lipid composition is key for narrow channels like gA, given that charged polar heads create an electric double layer in the channel mouths that enhances channel current[40] (note the change observed in the scaling behavior of gA from $G \sim c$ in Figure 2(a) to $G \sim c^0$ in Figure 2(b)). This effect should be secondary in wide pores with mouths comparable to the size of the double layer generated by lipid charges. However, a major role of the lipid charge is observed also in relatively large channels like Ala, CoV-E and specially OmpF (Figure 2(b) and Figure 3(a)), where diameter of channel mouths (including the protein walls) is larger than 4 nm.[34]

Here, we propose an interpretation for these results based on interfacial effects, specifically convergence resistance (also known as access resistance). The channel/solution interface may become the limiting step in ion conduction when the ion supply from the poorly conductive solution may not keep up with the demand of a crowded channel displaying high-rate transport.[49–51] This would happen in wide channels showing very effective permeation and not in narrow ones like gA where ion conduction is very poor.[40] Classic theory for this diffusion limitation predicts that convergence resistance should only depend on the size of the pore aperture and on bulk solution conductivity (Hall's equation),[52,53] even though it is a phenomenon occurring at the pore/solution interface. However, it has been recently demonstrated that charged lipids induce an accumulation of counterions near the channel mouth increasing local ion conductivity and hence lowering convergence resistance.[8] Analysis of Figure 2 and Figure 3 suggests that a surface property (lipid charge) exerts a certain modulation of a bulk effect (convergence resistance) showing how surface and bulk contributions are mutually interconnected.

Theoretical analysis of scaling arguments.

The conductance of nanopores has been typically described as the addition of bulk and surface contributions.[54,55] This treatment follows directly the analogy with glass capillaries where the surface conductance of a stagnant layer, physically separated from the rest of the fluid, is reported to be decisive.[54] However, such treatment presents at least two serious drawbacks, one conceptual and another operational. Firstly, no such surface-attached phase exists in aqueous membrane channels (ions just interchange their role and position continuously due to thermal agitation). Second, the bulk + surface model fails to reproduce the experimental results because no saturation of conductance is predicted at low salt concentration[55] (see Figure 2(b) and Figure 3). Alternative formulations have been proposed in the context of the Donnan description[7,8,20,55] which yield the following expression:

$$G = \left(\pi D^2 \kappa_b / 4L\right)\sqrt{\left(\rho_p / 2c\right)^2 + 1} \quad (1)$$

where ρ_p is the effective excess counterion concentration due to the protein charges; D and L are the pore diameter and length, respectively, and κ_b is the bulk conductivity. Equation (1) does not contain separate contributions for the bulk and surface conductances, but a single expression with two limiting cases for bulk- (ρ_p << c, G ~ c) and surface-controlled (ρ_p >> c, G ~ c^0) conductance. Intermediate exponents between c^0 and c^1 just reflect the transition from one regime to the other depending on the pore characteristics (ρ_p). Interestingly, recent approaches using the space-charge theory have stressed the limitations of the Donnan treatment at low c when the EDL overlaps and suggest the scaling G ~ $c^{0.5}$ for the surface-governed low concentration limit.[56] Exponents lower than 0.5 are explained invoking ion adsorption onto the pore surface via Langmuir isotherm.[20,56] However, our experiments with different lipid charges (Figure 2(a)) suggest that, at least in biological channels, deviations from equation (1) are probably not related to the limitations of the Donnan treatment[20,56] but due to overlooking interfacial effects. Access resistance can be added to equation (1) via Hall's equation but considering also that the effective excess counterion concentration due to lipid charges, ρ_l, changes the effective solution conductivity in the channel mouth:[8]

$$1/G = \left[\left(\pi D^2 \kappa_b / 4L\right)\sqrt{\left((\rho_p + \rho_l)/2c\right)^2 + 1}\right]^{-1} + \left(D\kappa_b\sqrt{\left(\rho_l/2c\right)^2 + 1}\right)^{-1} \quad (2)$$

Note that ρ_l also alters the channel proper conductance. By using equation (2), an excellent agreement between theory and experiments can be found in the case of OmpF channel.[8] Unfortunately, equation (2) has no such straightforward limiting cases as equation (1) because the effects from different factors (pore geometry, pore charge, and membrane charge) are closely interconnected. Anyway, some estimations about the dominating scaling factor can be made considering separately the roles of membrane and protein charges in equation (2).

First, we consider the case where lipid membranes are uncharged (ρ_l ~ 0). In the high concentration range, protein charge effects become negligible (ρ_p << c) so that both pore and

convergence conductance scale linearly with concentration. In the low concentration limit ($\rho_p >> c$), we can get some insight by considering that in the parallel arrangement of equation (2) both factors play a role when they are comparable:

$$\frac{\left(\pi D^2 \kappa_b / 4L\right)\sqrt{\left(\rho_p/2c\right)^2 + 1}}{D\kappa_b} \approx 1. \quad (3)$$

This leads to the following condition:

$$\frac{D}{L} \approx \frac{8c}{\pi\rho_p} \approx \frac{5c}{2\rho_p} \quad (4)$$

Considering typical values L ~ 5 nm and D ~ 1–2 nm, interfacial effects showing bulk-like scaling (G ~ c) are expected to appear in the millimolar low concentration limit provided that ρ_p > 100 mM, which is the case of all channels studied here except of gA. In the case of the uncharged gA we find an association between two terms that yields bulk-like scaling, which leads to G ~ c in any case. Interestingly, both low and high concentration scaling predictions based on equation (2) for uncharged membranes agree with the experiments reported in Figure 2(a).

The presence of charged membranes increases significantly both pore and interfacial conductance. In the high concentration limit both protein and lipid charge effects become negligible so that the overall conductance should scale linearly with concentration. For low c, assuming that $\rho_l \sim \rho_p$ (ρ_p is probably higher than ρ_l in some cases) and following a similar reasoning to that implicit in equation 3, the condition required for interfacial conductance to play a role is D/L ~ 2/π. For L = 5 nm this requires a pore diameter of D > 3 nm, which is wider than all the channels studied here, so that no interfacial effects should appear in Figure 2(b). Therefore, the conductance saturation observed at low concentrations arises from the pore conductance, which is controlled by the protein and lipid charges in order to preserve charge neutrality. The transition from high- to low-concentration occurs at concentrations comparable to ρ_p. For the case of gA, which again has zero net charge, the $G \sim c^0$ scaling appears in all concentration range probably because of its narrow entrances leading to extremely high lipid charge concentration ρ_l. This means that, in practice, the condition $\rho_l << c$ necessary to obtain linear scaling is not met in our experiments with gA.

Numerical calculation of conductance scaling.

To understand the origin of the dominant contributions to conductance scaling we use a three-dimensional Poisson–Nernst–Planck (PNP-3D) model[57] implemented as described in detail elsewhere.[58,59] We use the 3D atomic structure of gA and OmpF available at the

Protein Data Bank (codes 1JNO and 2OMF, respectively). Note that no structure is available for Ala or CoV-E proteolipidic pores. Given each protein structure, the channel fixed charge density was obtained to calculate the apparent pK_a of the channel residues. Ion fluxes and concentrations along the pore were calculated using bulk pH, salt concentrations, and electric potential at the channel entrances as boundary conditions. The existence of a charged membrane was simulated adding a small charged region over the ion inaccessible membrane region. Ion diffusion coefficients were introduced as free parameters. More details about the procedure are given as Supplementary Information.

Figure 4(a) and (b) show a good agreement between conductance calculations (*dashed lines*) and experimental data (*points*) for gA and OmpF in neutral (Figure 4(a)) and charged (Figure 4(b)) membranes, although the numerical model tends to overestimate the measured conductance, as previously reported.[60,61] Conductance scaling displays approximate bulk conduction in neutral membranes ($G \sim c^{0.7}$, Figure 4(a)), while membrane charge reveals surface conduction in the low concentration regime ($G \sim c^0$, Figure 4(b)). According to the scaling arguments mentioned before, the transition between bulk and surface conduction should occur around ρ_p. Calculations in Figure 4 (b) show that in the case of OmpF, conductance scaling changes close to 0.1 M, which actually corresponds to the average protein charge density of the channel reported in previous studies.[30] In practice, this means that ion concentration inside the channel is regulated by surface pore charges due to electroneutrality requirements, so that extremely diluted bulk solutions do not imply low pore conductance because surface conduction prevails. Conversely, very concentrated solutions screen the channel charges so effectively that pore selectivity is “salted-out” and bulk conductance is observed.[30]

We have computed the profile of the equilibrium electric potential (for zero current) along the channel + membrane system for OmpF (Figure 4(c)) and gA (Figure 4(d)), in the low salt regime (c = 5 mM) where charge effects become apparent. For neutral membranes, the potential well in the case of gA is almost two-fold deeper than in OmpF, which agrees with the well-known ideal selectivity of gA and the relatively weaker ion charge discrimination of OmpF.[30,40,62] The potential drop in gA is confined to the inner part of the pore, whereas for OmpF a remarkable fraction of the total potential drop occurs in interfacial regions due to the presence of charged residues near the channel mouths.[30] In both channels charged membranes enhance the potential well across the channel itself pointing to an increase in pore conductance, as interpreted in the previous section. Charged lipids, actually surrounding channel mouths, broaden the potential well (especially in the case of gA) so that a significant part of the equilibrium voltage falls into the solution. Note that carrier accumulation by lipid charges in OmpF is not significant because this effect is already induced by charged residues in the pore mouths.

Next, the non-equilibrium performance of the channel is analyzed. The profile of applied potential is obtained by subtraction of the equilibrium potential from the overall potential under an externally applied voltage of 100 mV. Note that interfacial effects will be caused by any applied potential drop falling outside the pore. The profile of applied potential is shown for OmpF (Figure 4(e)) and gA (Figure 4(f)). Figure 4(f) demonstrates that for gA interfacial effects are negligible in any case because almost 90% of the total drop occurs in the pore

itself regardless of the lipid charge. In contrast, interfacial effects are significant in OmpF and depend crucially on the membrane charge (45% of the total drop falls outside the channel in neutral membranes in contrast to 28% in charged ones for the conditions depicted in Figure 4(e)).

In summary, detailed numerical calculations performed in the two channels with available 3D structure confirm the trends anticipated by inspection of scaling behavior discussed in the previous section. Interfacial effects (lipid charges) manage to regulate the total conductance of either narrow or wide channels by using different mechanisms: in the intrinsically conductive OmpF they just control the access resistance and, in contrast, in the highly resistive gA they increase pore conductance by accumulation of carriers.

Concluding remarks.

Experiments performed in protein channels show a variety of scaling behaviors in the G(c) dependence as a result of the existence of competing mechanisms. We show that power laws are not an intrinsic feature of any of the channels studied, but they are a strong function of multiple factors like solution concentration, pH and membrane charge. This suggests that the diversity of scaling laws reported in the literature for similar systems probably arises from different outcomes on the balance of the contending mechanisms. Simple scaling arguments can explain satisfactorily most of the experimental findings provided that all contributing factors are considered. We have shown that competing mechanisms could display similar scaling behavior, or the dominating mechanism could mask the presence of others, leading to wrong conclusions. In particular, we show that the apparent universal scaling found in biological channels with dissimilar characteristics appears because interfacial effects depending on solution conductivity dominate. The use of atomic 3D structure-based PNP formalism provides calculations in line with experiments and validates scaling arguments. The found agreement underscores the usefulness of scaling qualitative arguments as diagnostic tools in systems where the actual structure is unknown such as proteolipidic channels or inhomogeneous abiotic nanopores.

Supplementary Material

Refer to Web version on PubMed Central for supplementary material.

ACKNOWLEDGMENTS

M.Q.M. was supported by the Intramural Research Program of the National Institutes of Health, *Eunice Kennedy Shriver* National Institute of Child Health and Human Development (Bethesda, MD, USA). M.L.L., M.A.A., V.M.A. and A.A. acknowledge financial support from the Spanish Government (FIS2016–75257-P AEI/FEDER) and Universitat Jaume I (P1.1B2015–28). M.Q.M. thanks Sergey M. Bezrukov (NIH, Bethesda, MD, USA) for his support and advice during the development of this work.

REFERENCES

(1). Luo ZX; Xing YZ; Ling YC; Kleinhammes A; Wu Y Electroneutrality Breakdown and Specific Ion Effects in Nanoconfined Aqueous Electrolytes Observed by NMR. Nat. Commun 2015, 6, 1–8.

(2). López ML; Queralt-Martín M; Alcaraz A Experimental Demonstration of Charge Inversion in a Protein Channel in the Presence of Monovalent Cations. Electrochem. commun 2014, 48, 32–34.

(3). He Y; Gillespie D; Boda D; Vlassiouk I; Eisenberg RS; Siwy ZS Tuning Transport Properties of Nanofluidic Devices with Local Charge Inversion. J. Am. Chem. Soc 2009, 131 (14), 5194–5202. [PubMed: 19317490]

(4). Alcaraz A; Ramírez P; García-Giménez E; López ML; Andrio A; Aguilella VM A pH-Tunable Nanofluidic Diode: Electrochemical Rectification in a Reconstituted Single Ion Channel. J. Phys. Chem. B 2006, 110 (42), 21205–21209. [PubMed: 17048946]

(5). Ramírez P; Gómez V; Cervera J; Schiedt B; Mafé S Ion Transport and Selectivity in Nanopores with Spatially Inhomogeneous Fixed Charge Distributions. J. Chem. Phys 2007, 126 (19), 194703. [PubMed: 17523824]

(6). Pang P; He J; Park JH; Krstić PS; Lindsay S; Krsti PS; Lindsay S; Krstić PS; Lindsay S; Krsti PS; et al. Origin of Giant Ionic Currents in Carbon Nanotube Channels. ACS Nano 2011, 5 (9), 7277–7283. [PubMed: 21888368]

(7). Bocquet L; Charlaix E Nanofluidics, from Bulk to Interfaces. Chem. Soc. Rev 2010, 39 (3), 1073–1095. [PubMed: 20179826]

(8). Alcaraz A; López ML; Queralt-Martín M; Aguilella VM Ion Transport in Confined Geometries below the Nanoscale: Access Resistance Dominates Protein Channel Conductance in Diluted Solutions. ACS Nano 2017, 11 (10), 10392–10400. [PubMed: 28930428]

(9). Malgaretti P; Pagonabarraga I; Rubi JM Entropic Transport in Confined Media: A Challenge for Computational Studies in Biological and Soft-Matter Systems. Front. Phys 2013, 1 (November), 1–9.

(10). Berezhkovskii AM; Bezrukov SM On the Applicability of Entropy Potentials in Transport Problems. Eur. Phys. J. Spec. Top 2014, 223 (14), 3063–3077. [PubMed: 26339466]

(11). Duan C; Majumdar A Anomalous Ion Transport in 2-Nm Hydrophilic Nanochannels. Nat. Nanotechnol 2010, 5 (12), 848–852. [PubMed: 21113159]

(12). Wautelet M Scaling Laws in the Macro-, Micro- and Nanoworlds. Eur. J. Phys 2001, 22 (6), 601–611.

(13). Corral Á; Ossó A; Llebot JE Scaling of Tropical-Cyclone Dissipation. Nat. Phys 2010, 6 (9), 693–696.

(14). Gazzola M; Argentina M; Mahadevan L Scaling Macroscopic Aquatic Locomotion. Nat. Phys 2014, 10 (10), 758–761.

(15). Mantegna RN; Stanley HE Scaling Behaviour in the Dynamics of an Economic Index. Nature 1995, 376 (6535), 46–49.

(16). Stanley MHR; Amaral LAN; Buldyrev SV; Havlin S; Leschhorn H; Maass P; Salinger MA; Stanley HE Scaling Behaviour in the Growth of Companies. Nature 1996, 379 (6568), 804–806.

(17). Likens AD; Fine JM; Amazeen EL; Amazeen PG Experimental Control of Scaling Behavior: What Is Not Fractal? Exp. Brain Res 2015, 233 (10), 2813–2821. [PubMed: 26070902]

(18). Rybski D; Buldyrev SV; Havlin S; Liljeros F; Makse HA Scaling Laws of Human Interaction Activity. Proc. Natl. Acad. Sci 2009, 106 (31), 12640–12645. [PubMed: 19617555]

(19). Amiri H; Shepard KL; Nuckolls C; Hernández Sánchez R Single-Walled Carbon Nanotubes: Mimics of Biological Ion Channels. Nano Lett 2017, 17 (2), 1204–1211. [PubMed: 28103039]

(20). Secchi E; Niguès A; Jubin L; Siria A; Bocquet L Scaling Behavior for Ionic Transport and Its Fluctuations in Individual Carbon Nanotubes. Phys. Rev. Lett 2016, 116 (15), 154501. [PubMed: 27127970]

(21). Lev AA; Korchev YE; Rostovtseva TK; Bashford CL; Edmonds DT; Pasternak CA Rapid Switching of Ion Current in Narrow Pores: Implications for Biological Ion Channels. Proceedings. Biol. Sci 1993, 252 (1335), 187–192.

(22). Stein D; Kruithof M; Dekker C Surface-Charge-Governed Ion Transport in Nanofluidic Channels. Phys. Rev. Lett 2004, 93 (3), 035901. [PubMed: 15323836]

(23). Wang S; Li H; Sawada H; Allen CS; Kirkland AI; Grossman JC; Warner JH Atomic Structure and Formation Mechanism of Sub-Nanometer Pores in 2D Monolayer MoS 2. Nanoscale 2017, 9 (19), 6417–6426. [PubMed: 28463370]

(24). Suk ME; Aluru NR Water Transport through Ultrathin Graphene. J. Phys. Chem. Lett 2010, 1 (10), 1590–1594.

(25). O'Hern SC; Stewart CA; Boutilier MSH; Idrobo J-C; Bhaviripudi S; Das SK; Kong J; Laoui T; Atieh M; Karnik R Selective Molecular Transport through Intrinsic Defects in a Single Layer of CVD Graphene. ACS Nano 2012, 6 (11), 10130–10138. [PubMed: 23030691]

(26). Zhao Y; Xie Y; Liu Z; Wang X; Chai Y; Yan F Two-Dimensional Material Membranes: An Emerging Platform for Controllable Mass Transport Applications. Small 2014, 10 (22), 4521–4542. [PubMed: 25207987]

(27). Plesa C; Kowalczyk SW; Zinsmeester R; Grosberg AY; Rabin Y; Dekker C Fast Translocation of Proteins through Solid State Nanopores. Nano Lett 2013, 13 (2), 658–663. [PubMed: 23343345]

(28). Merchant CA; Healy K; Wanunu M; Ray V; Peterman N; Bartel J; Fischbein MD; Venta K; Luo Z; Johnson ATC; et al. DNA Translocation through Graphene Nanopores. Nano Lett 2010, 10 (8), 2915–2921. [PubMed: 20698604]

(29). Andersen OS; Koeppe II RE; Roux B Gramicidin Channels: Versatile Tools In Biological Membrane Ion Channels; Springer New York: New York, NY, 2007; pp 33–80.

(30). Alcaraz A; Nestorovich EM; Aguilella-Arzo M; Aguilella VM; Bezrukov SM Salting out the Ionic Selectivity of a Wide Channel: The Asymmetry of OmpF. Biophys. J 2004, 87 (2), 943–957. [PubMed: 15298901]

(31). Alcaraz A; Nestorovich EM; López ML; García-Giménez E; Bezrukov SM; Aguilella VM Diffusion, Exclusion, and Specific Binding in a Large Channel: A Study of OmpF Selectivity Inversion. Biophys. J 2009, 96 (1), 56–66. [PubMed: 19134471]

(32). Rostovtseva TK; Nestorovich EM; Bezrukov SM Partitioning of Differently Sized Poly(Ethylene Glycol)s into OmpF Porin. Biophys. J 2002, 82 (1 Pt 1), 160–169. [PubMed: 11751305]

(33). Cowan SW Bacterial Porins: Lessons from Three High-Resolution Structures. Curr. Opin. Struct. Biol 1993, 3 (4), 501–507.

(34). Cowan SW; Schirmer T; Rummel G; Steiert M; Ghosh R; Pauptit R. a; Jansonius JN; Rosenbusch JP Crystal Structures Explain Functional Properties of Two E. Coli Porins. Nature 1992, 358 (6389), 727–733. [PubMed: 1380671]

(35). Aguilella VM; Bezrukov SM Alamethicin Channel Conductance Modified by Lipid Charge. Eur. Biophys. J 2001, 30 (4), 233–241. [PubMed: 11548125]

(36). Woolley GA Channel-Forming Activity of Alamethicin: Effects of Covalent Tethering. Chem. Biodivers 2007, 4 (6), 1323–1337. [PubMed: 17589884]

(37). Verdiá-Báguena C; Nieto-Torres JL; Alcaraz A; DeDiego ML; Torres J; Aguilella VM; Enjuanes L Coronavirus E Protein Forms Ion Channels with Functionally and Structurally-Involved Membrane Lipids. Virology 2012, 432 (2), 485–494. [PubMed: 22832120]

(38). Verdiá-Báguena C; Nieto-Torres JL; Alcaraz A; DeDiego ML; Enjuanes L; Aguilella VM Analysis of SARS-CoV E Protein Ion Channel Activity by Tuning the Protein and Lipid Charge. Biochim. Biophys. Acta - Biomembr 2013, 1828 (9), 2026–2031.

(39). Aguilella VM; Verdiá-Báguena C; Alcaraz A Lipid Charge Regulation of Non-Specific Biological Ion Channels. Phys. Chem. Chem. Phys 2014, 16 (9), 3881–3893. [PubMed: 24452437]

(40). Rostovtseva TK; Aguilella VM; Vodyanoy I; Bezrukov SM; Parsegian VA Membrane Surface-Charge Titration Probed by Gramicidin A Channel Conductance. Biophys. J 1998, 75 (4), 1783–1792. [PubMed: 9746520]

(41). Kelkar DA; Chattopadhyay A The Gramicidin Ion Channel: A Model Membrane Protein. Biochim. Biophys. Acta - Biomembr 2007, 1768 (9), 2011–2025.

(42). Corry B; Chung S-H Mechanisms of Valence Selectivity in Biological Ion Channels. Cell. Mol. Life Sci 2006, 63 (3), 301–315. [PubMed: 16389453]

(43). Roux B Computational Studies of the Gramicidin Channel. Acc. Chem. Res 2002, 35 (6), 366–375. [PubMed: 12069621]

(44). Andersen OS Ion Movement through Gramicidin A Channels. Single-Channel Measurements at Very High Potentials. Biophys. J 1983, 41 (2), 119–133. [PubMed: 6188500]

(45). Andersen OS Ion Movement through Gramicidin A Channels. Interfacial Polarization Effects on Single-Channel Current Measurements. Biophys. J 1983, 41 (2), 135–146. [PubMed: 6188501]

(46). Andersen OS Ion Movement through Gramicidin A Channels. Studies on the Diffusion-Controlled Association Step. Biophys. J 1983, 41 (2), 147–165. [PubMed: 6188502]

(47). Eisenberg M; Hall JE; Mead CA The Nature of the Voltage-Dependent Conductance Induced by Alamethicin in Black Lipid Membranes. J. Membr. Biol 1973, 14 (1), 143–176. [PubMed: 4774545]

(48). Tyäuble H; Teubner M; Woolley P; Eibl H Electrostatic Interactions at Charged Lipid Membranes. I. Effects of pH and Univalent Cations on Membrane Structure. Biophys. Chem 1976, 4 (4), 319–342. [PubMed: 8167]

(49). Läuger P Diffusion-Limited Ion Flow through Pores. Biochim. Biophys. Acta - Biomembr 1976, 455 (2), 493–509.

(50). Apell HJ; Bamberg E; Läuger P Effects of Surface Charge on the Conductance of the Gramicidin Channel. Biochim. Biophys. Acta 1979, 552 (3), 369–378. [PubMed: 87221]

(51). Kuno M; Ando H; Morihata H; Sakai H; Mori H; Sawada M; Oiki S Temperature Dependence of Proton Permeation through a Voltage-Gated Proton Channel. J. Gen. Physiol 2009, 134 (3), 191–205. [PubMed: 19720960]

(52). Hall JE Access Resistance of a Small Circular Pore. J. Gen. Physiol 1975, 66 (4), 531–532. [PubMed: 1181379]

(53). Bezrukov SM; Vodyanoy I Probing Alamethicin Channels with Water-Soluble Polymers. Effect on Conductance of Channel States. Biophys. J 1993, 64 (1), 16–25. [PubMed: 7679295]

(54). Schoch RB; Renaud P Ion Transport through Nanoslits Dominated by the Effective Surface Charge. Appl. Phys. Lett 2005, 86 (25), 1–3.

(55). Lee C; Joly L; Siria A; Biance A-L; Fulcrand R; Bocquet L Large Apparent Electric Size of Solid-State Nanopores Due to Spatially Extended Surface Conduction. Nano Lett 2012, 12 (8), 4037–4044. [PubMed: 22746297]

(56). Biesheuvel PM; Bazant MZ Analysis of Ionic Conductance of Carbon Nanotubes. Phys. Rev. E 2016, 94 (5), 050601. [PubMed: 27967121]

(57). Kurnikova MG; Coalson RD; Graf P; Nitzan A A Lattice Relaxation Algorithm for Three-Dimensional Poisson-Nernst-Planck Theory with Application to Ion Transport through the Gramicidin A Channel. Biophys. J 1999, 76 (2), 642–656. [PubMed: 9929470]

(58). Queralt-Martín M; Peiró-González C; Aguilella-Arzo M; Alcaraz A Effects of Extreme pH on Ionic Transport through Protein Nanopores: The Role of Ion Diffusion and Charge Exclusion. Phys. Chem. Chem. Phys 2016, 18 (31), 21668–21675. [PubMed: 27464527]

(59). Aguilella-Arzo M; Queralt-Martín M; Lopez M-LM-L; Alcaraz A Fluctuation-Driven Transport in Biological Nanopores. A 3D Poisson–Nernst–Planck Study. Entropy 2017, 19 (3), 116.

(60). Roux B; Allen T; Bernèche S; Im W Theoretical and Computational Models of Biological Ion Channels. Q. Rev. Biophys 2004, 37 (1), 15–103. [PubMed: 17390604]

(61). Ramírez P; Aguilella-Arzo M; Alcaraz A; Cervera J; Aguilella VM Theoretical Description of the Ion Transport across Nanopores with Titratable Fixed Charges: Analogies between Ion Channels and Synthetic Pores. Cell Biochem. Biophys 2006, 44 (2), 287–312. [PubMed: 16456229]

(62). Aguilella VMVM; Queralt-Martín M; Aguilella-Arzo M; Alcaraz A Insights on the Permeability of Wide Protein Channels: Measurement and Interpretation of Ion Selectivity. Integr. Biol 2011, 3 (3), 159–172.

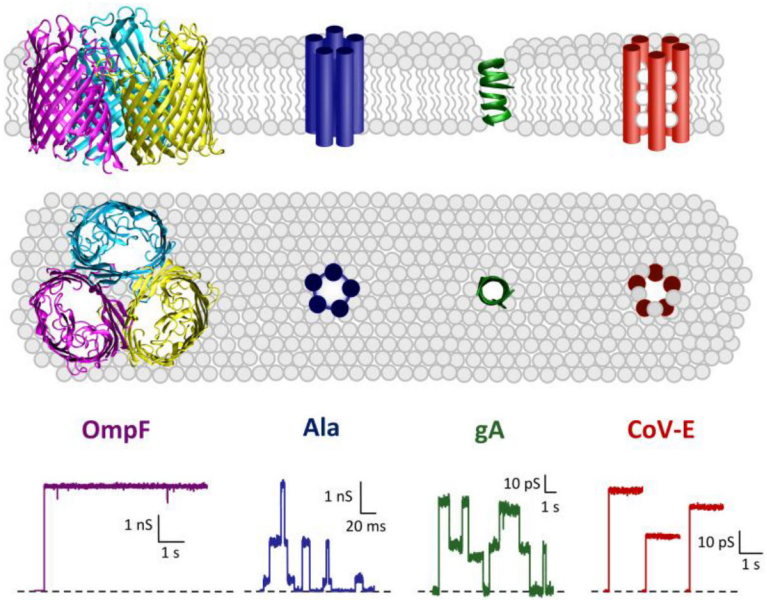

Figure 1. Structure and current traces of the different channels studied.

Cartoons representing the channel structures show a lateral view in the upper panel and a top view in the middle panel. OmpF and gA are represented with their resolved three-dimensional structures (PDB codes 2OMF and 1JNO, respectively), while Ala and CoV-E display cylinders exemplifying monomers conforming a putative oligomeric state. In the lower panel, representative current traces of each channel are displayed at 1 M KCl concentration in neutral lipid. More detailed traces and technical information are shown in Figure S1.

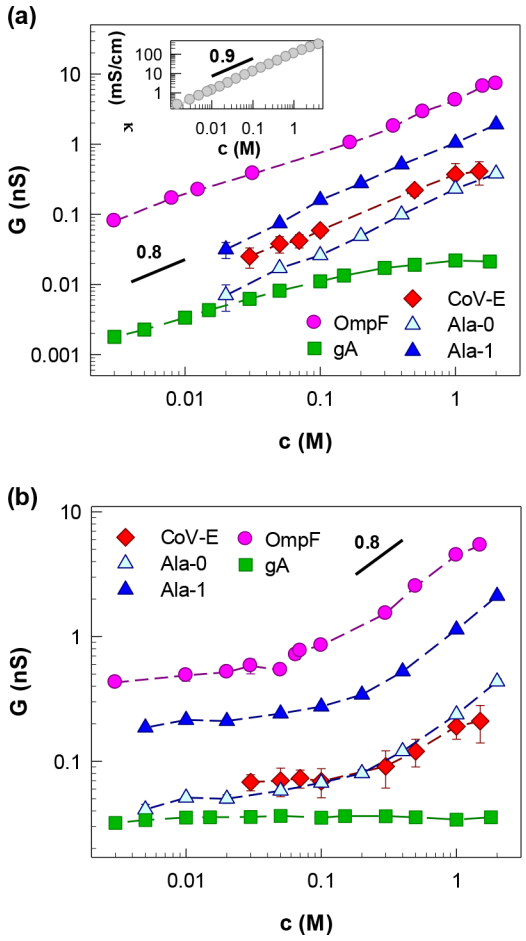

Figure 2. Conductance scaling with salt concentration.

Single-channel conductance G = I/V measured across different biological pores inserted in a neutral (a) or charged (b) membrane, for a wide range of symmetrical KCl concentrations at pH 6. Applied voltage was always 100 mV, except for Ala conductance which was recorded at 140 mV. Inset in (a) displays the measured conductivity in the same range of KCl concentrations. Solid lines correspond to equation $G \sim c^{\alpha}$, with α displayed next to each line. Dashed lines are drawn to guide the eye. Data are means of at least three independent experiments ± S.D. (when not visible, error bars are smaller than symbol size).

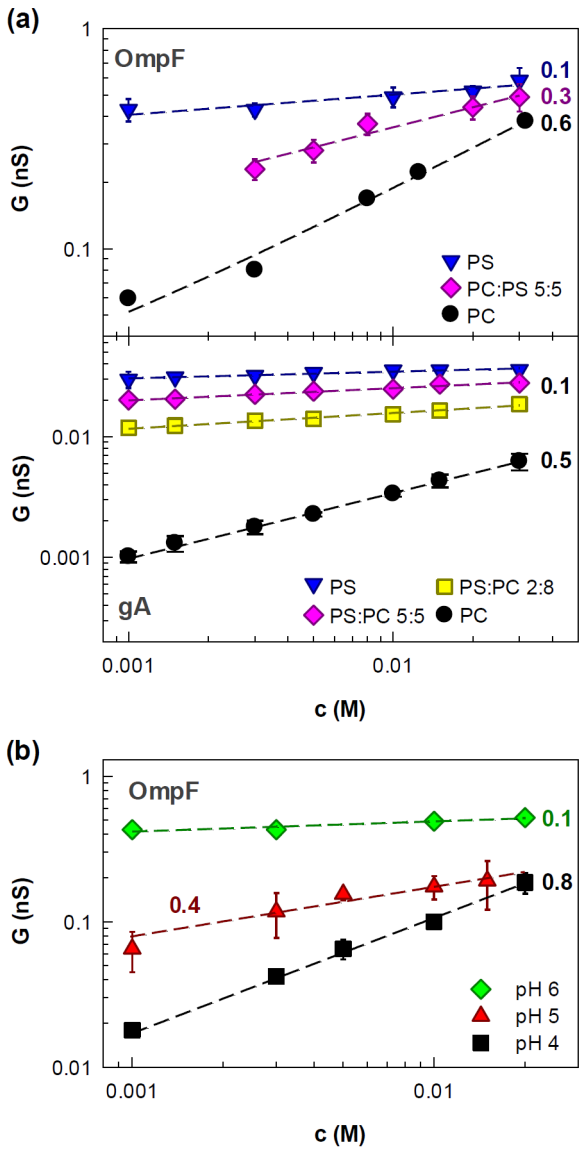

Figure 3. Effect of membrane and channel charge on conductance scaling.

(a) Single-channel conductance G measured at pH = 6 for different salt concentrations across OmpF (*upper panel*) or gA (*lower panel*) inserted in different membranes with varying ratios of neutral (DPhPC) and charged (DPhPS) lipid, as indicated. (b) Single-channel conductance as a function of salt concentration measured for OmpF inserted in a charged membrane (DPhPS) under different solution pH, as indicated. In (a) and (b), the applied voltage was 100 mV; dashed lines correspond to fitting to equation $G \sim c^{\alpha}$, with α displayed next to each line; data are averages of at least three independent experiments ± S.D.

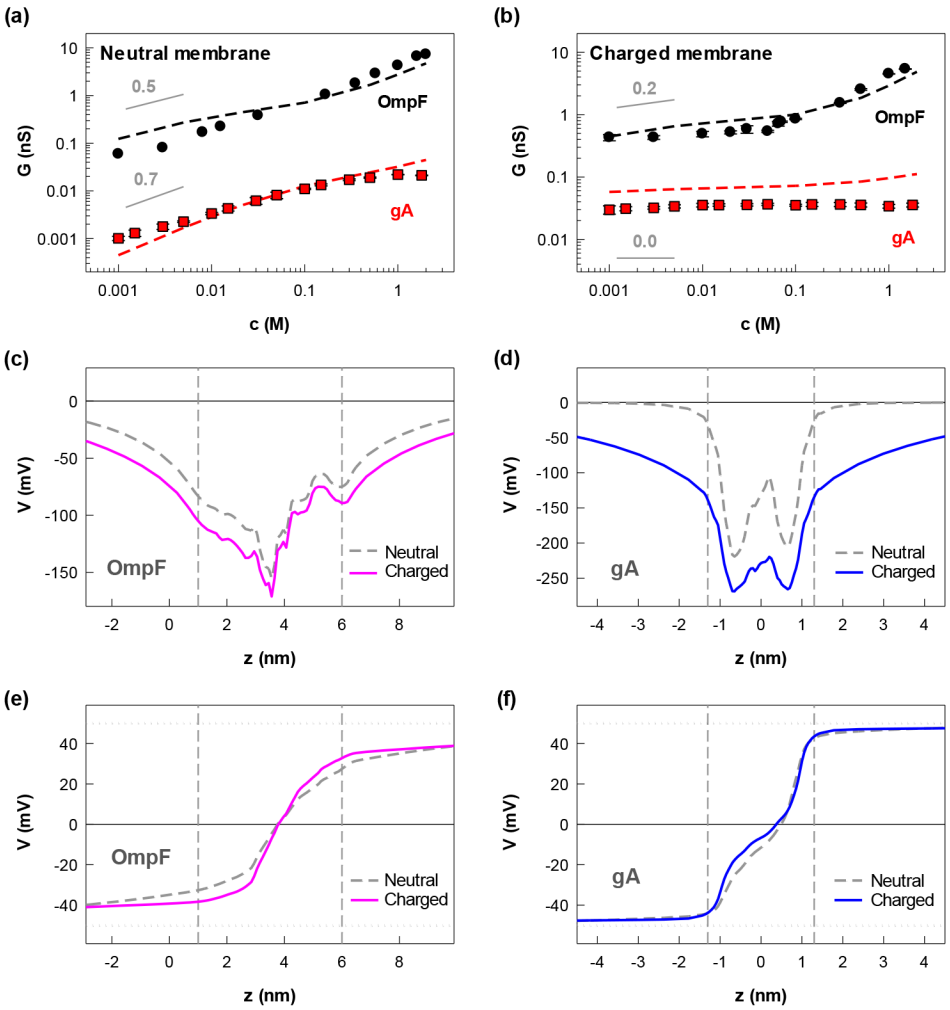

Figure 4. Numerical calculations obtained from the PNP-3D model.

(a)-(b) Experimental (*points*) and calculated (dashed *lines*) single-channel conductance G scaling with concentration c across OmpF or gA, as indicated, inserted in a neutral DPhPC (a) or charged DPhPS (b) membrane. Applied voltage in calculations was 100 mV. Solid lines correspond to equation $G \sim c^{\alpha}$, with α displayed next to each line. (c)-(f) Theoretical predictions for the equilibrium ((c) and (d)) and applied ((e) and (f)) potential profiles in OmpF or gA inserted in a neutral or charged membrane, as indicated. Vertical dashed lines correspond approximately to the location of channel mouths. KCl salt concentration used is 5 mM. In (e) and (f), horizontal dotted lines indicate the value of the applied potential on both solutions (from −50 mV to +50 mV, ΔV = 100 mV).